Chemical Engineering Journal 232 (2013) 139–148

Contents lists available at ScienceDirect

Chemical Engineering Journal

journal homepage: www.elsevier.com/locate/cej

CO_2 capture with a novel solid fluidizable sorbent: Thermodynamics and Temperature Programmed Carbonation–Decarbonation

Muhammad B.I. Chowdhury, Mohammad R. Quddus, Hugo I. deLasa *

[a] Department of Chemical and Biochemical Engineering, Western University, London, ON N6G 5B9, Canada

HIGHLIGHTS

- We prepared a new and stable CO_2 sorbent based on lithium orthosilicate.
- We develop a CO_2 capture thermodynamic analysis for various fluidizable sorbents.
- We develop TPC and TPDC using a temperature programmed fixed bed unit.
- We develop TPC–TPDC runs using calcium carbonate and lithium orthosilicate.
- We are able to predict sorbent regeneration and temperature inversion points.

GRAPHICAL ABSTRACT

Consecutive CO_2 absorption–desorption with the new fluidizable Li_4SiO_4. Temperature ramp: 5 °C/min; Input Gas composition: 10 vol% CO_2 in helium; flow rate: 50 mL/min.

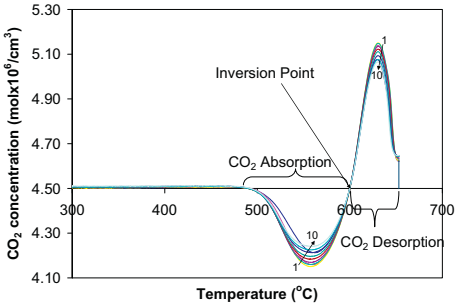

ARTICLE INFO

Article history:
Received 24 April 2013
Received in revised form 15 July 2013
Accepted 17 July 2013
Available online 27 July 2013

Keywords:
CO_2 capture
Fluidizable sorbents
Thermodynamics
Temperature Programmed Carbonation
Temperature Programmed Decarbonation

ABSTRACT

This study investigates several sorbents for CO_2 capture with emphasis on the development of a novel lithium orthosilicate based sorbent. Thermodynamic analysis is considered to predict sorbent regeneration conditions and thermal levels where sorbent kinetics change from CO_2 absorption to CO_2 desorption. Temperature Programmed Carbonation (TPC) and Temperature Programmed Decarbonation (TPDC) are developed using a temperature programmed fixed bed unit. Sorbents are kept in contact with a gas stream containing a 10% CO_2 mole fraction, and are subjected to a 5 °C/min temperature ramp. Calcium carbonate, lithium orthosilicate and a novel lithium orthosilicate modified sorbent are considered for these runs. TPC–TPDC runs confirm thermodynamic predictions for thermal inversion points. Furthermore, TPD–TPDC runs show that the novel lithium orthosilicate based sorbent provides a very stable and increased CO_2 sorption capacity over 10 absorption–regeneration cycles, while calcium carbonate displays a reduced CO_2 sorption capacity with cyclic operation. This fluidizable novel sorbent can significantly contribute towards CO_2 removal from flue gases emitted by power plants.

1. Introduction

Global warming by increasing anthropogenic emissions of greenhouse gases is important in the world today. These emissions, which are mainly carbon dioxide, must be mitigated to minimize the on-going irreversible environmental damages. The concentrations of carbon dioxide have increased from 280 ppm in the pre-industrial age to more than 380 ppm today. In fact, they increase by more than 2 ppm per year [1]. Thus, novel technologies are required to capture carbon dioxide and to store it.

In this respect, CO_2 removal from large stationary emission sources such as power plants should be, especially targeted. Stationary sources release approximately half of the global CO_2 emissions. One of the most viable techniques for CO_2 capture is chemical absorption using a solid sorbent. Calcite, dolomite,

* Corresponding author. Tel.: +1 (519) 661 2144; fax: +1 (519) 661 3498.
E-mail address: hdelasa@eng.uwo.ca (H.I. deLasa).

1385-8947/$ - see front matter © 2013 Elsevier B.V. All rights reserved.
http://dx.doi.org/10.1016/j.cej.2013.07.044

Nomenclature

a_i	activity coefficient for the "i" chemical species i
C	CO_2 concentration in the gas exiting stream (mol/cm^3)
C_0	CO_2 concentration in the incoming stream (mol/cm^3)
C_p	heat capacity (J/mol-K)
f_i	fugacity of chemical species i (bar)
K	equilibrium reaction constant
P_{rxn}	total reaction pressure (bar)
p_i	partial pressure of species i (bar)
p_{CO_2}	partial pressure of carbon dioxide (bar)
R	universal gas constant (8.314 J/mol-K)
T	temperature (K)
y_i	mole fraction of species i

Greek Symbols

ΔG°	standard Gibbs Free Energy change (kJ/mol)
ΔG_{rxn}	change of Gibbs Free Energy of reaction (kJ/mol)
ΔH°	standard enthalpy change (kJ/mol)
Φ_i	fugacity co-efficient of chemical species i
v_i	stoichiometric co-efficient of species i

Sorbent designation

Calcite $CaCO_3$ (99%)
Limestone (Cadomin 1) CaO (54%)
Lithium orthosilicate Li_4SiO_4 (99.9%)
Lithium zirconate Li_2ZrO_3 (94%)
Sodium silicate Na_2SiO_3

lithium ceramics are gaining attention for large scale CO_2 capture via this type of process. In this process, CO_2 reacts with solid sorbents producing metal carbonates and/or metal oxides or silicates.

$$CaO + CO_2 \Longleftrightarrow CaCO_3 \quad (1)$$

$$Li_2ZrO_3 + CO_2 \Longleftrightarrow Li_2CO_3 + ZrO_2 \quad (2)$$

$$Li_4SiO_4 + CO_2 \Longleftrightarrow Li_2CO_3 + Li_2SiO_3 \quad (3)$$

$$Na_2SiO_3 + CO_2 \Longleftrightarrow Na_2CO_3 + SiO_2 \quad (4)$$

These sorbents can be thermally regenerated by heating the metal carbonate beyond the carbonation temperature. Under these conditions, the regeneration or reverse of reactions (1)–(4) are allowed.

Thus, solid sorbents can be used in principle for CO_2 capture if carbonation may be achieved at flue gas conditions. Furthermore, metal carbonates decomposition temperatures are equally important. For instance, metal carbonates requiring more than 1000 °C may not be suitable for this process, as they require extra supply of energy and costly equipment [2].

It is envisioned that the chemical looping cycle using fluidized bed units could involve two interconnected fluidized beds treating the exhaust of power stations. This configuration facilitates the reversible CO_2 adsorption and desorption process. Therefore, at the outlet of the system an essentially pure stream of CO_2 is produced, ready for geological sequestration. Major advantages of this technology are that it uses high-temperatures and can be implemented in large-scale fluidized bed reactors. Given the existing knowledge with fluidized bed reactor engineering, it is expected the migration of this process from a lab-scale prototype to a pilot plant-scale or commercial scale unit can be accomplished relatively easily [3,4].

As a result, an actual industrial installation would consist of a cycling looping process involving a "carbonation reactor" and a "decarbonation reactor". However, the choice of specific sorbent would depend on the range of carbonation and decarbonation temperatures, the reactivity of the particular sorbent and its stability under cyclic operation [5].

One can notice from Eqs. (2)–(4) that some sorbents produce metal oxides and/or silicates, in addition to carbonates. Therefore, both various chemical and physical properties of the formed species have to be considered in the case of cyclical sorbent applications. For example, the melting point of Li_2CO_3 is 720 °C. Therefore, the operation of Li_2CO_3 has to be limited to 720 °C.

CO_2 capture using calcium oxide has been widely studied [2,10,11]. There are two possible rate-controlling steps influencing the gas–solid CaO–CO_2 reaction. The first step involves a rapid heterogeneous chemical reaction, while the second step consists of a slow CO_2 and CaO reaction resulting in the formation of a $CaCO_3$ layer [2,11]. This $CaCO_3$ layer considerably limits the access to unreacted CaO for further carbonation. Therefore, the reactivity of calcite decreases over the carbonation–decarbonation cycles.

In contrast, lithium zirconate and lithium orthosilicate are claimed to be stable even after 100 cycles [11]. Recent studies showed the potential of CO_2 capture using lithium zirconate [6–8] and lithium orthosilicate [9]. Kato et al. observed that Li_4SiO_4 absorb CO_2 at a faster rate than Li_2ZrO_3 at the same sorption conditions [12]. From the calculated relationship of the chemical potential of the CO_2 capture reaction as a function of temperatures and CO_2 partial pressures, Li_4SiO_4 appears to be a good candidate for high temperature CO_2 capture[13]. In addition, Li_4SiO_4 shows lower costs of the raw materials involved. This is the case when comparing the expensive ZrO_2 with the less costly SiO_2 [12].

Seggiani et al. doped Li_4SiO_4 with potassium and found that the sorption capacity increased as function of temperature between 500 °C and 580 °C [14]. However, above 580 °C, the sorption capacity decreased. Wang et al. developed a Li_4SiO_4-based sorbent using waste materials like rice husk ash (RHA) [15]. These authors found that metals in RHA doped with Li_4SiO_4 inhibit particle growth and increase pore volume and surface area. In addition, RHA doped with Li_4SiO_4 maintains its high CO_2 capacity during multiple cycles compared to pure Li_4SiO_4 [15]. Olivares-Marín et al. synthesized lithium based sorbent from fly ash in the presence of Li_2CO_3 at 950 °C. These authors found that CO_2 capture was a function of added K_2CO_3 [16].

CO_2 chemisorption using lithium based ceramics is controlled by different factors. Zhang et al. studied CO_2 sorption/desorption kinetics with Li_4SiO_4. These author found that in the sorption process, the CO_2 molecules come into contact with the sorbents and rapidly react to form a double-shell structure consisting of Li_2CO_3 and Li_2SiO_3 [17]. Initially, CO_2 chemisorption is controlled by the reactivity of the lithium ceramics [17,18] and the flow of CO_2 [19]. However, once the external lithium shell is produced at the lithium ceramic particle outer surface, the whole process may become diffusionally controlled[17–19].

It is thus concluded that an ideal sorbent being used in a cyclical system capturing CO_2 from hot flue gases, requires properties of both good CO_2 absorption–desorption capacity and high temperature stability. To address this issue, this research focuses on the development of a novel and stable lithium orthosilicate based sorbent, with enhanced structural properties to minimize CO_2 absorption/desorption diffusional limitations. The aim of this study is also to determine the best conditions for CO_2 capture; with these

conditions being identified on the basis of both carbonation–decarbonation thermodynamics and kinetics.

2. Thermodynamics at reaction equilibrium

Thermodynamics allow establishing the dependence of equilibrium constants on temperature and pressure [20]. One can thus, assess how operating conditions may influence CO_2 capture at chemical equilibrium.

2.1. Effect of temperature on chemical equilibrium constants

At reaction equilibrium, the CO_2 molar function is a variable function of both temperature and pressure. At a constant pressure, the dependence of ΔG° on T is given by the Gibbs–Helmholtz equation as follows [20],

$$\left[\frac{d(\Delta G^\circ/RT)}{dT}\right]_p = \frac{-\Delta H^\circ}{RT^2} \tag{7}$$

where R is a universal gas constant and T is the temperature. Both ΔG° and ΔH° are affected by pressure. At 1 atm or 1 bar standard condition Eq. (7) can be represented as:

$$\frac{d(\Delta G^\circ/RT)}{dT} = \frac{-\Delta H^\circ}{RT^2} \tag{8}$$

2.2. Effect of pressure on chemical equilibrium constants

The effect of pressure on chemical equilibrium can be formulated by applying Le Chatelier's principle. As a result, the equilibrium constant, K, of a heterogeneous reaction can be expressed as follows [20]

$$K(T) = \prod_{i=1} a_i^{\nu_i} = \frac{a_p^\rho \cdot a_q^\sigma \cdots}{a_x^\alpha a_y^\beta \cdots} \tag{9}$$

where K is the equilibrium constant, a_i is the activity coefficient and ν_i is the stoichiometric coefficient of the species i. While activity coefficients for solids are set to 1. For gases, activity coefficients are defined as the ratio of the species fugacity in the mixture to the fugacity at its standard state,

$$a_i = \frac{\bar{f}_i}{\bar{f}_i^o} \tag{10}$$

with $\bar{f}_i^o = P_o$ = 1 bar or 1 atm, defining the gas species at the standard state:

Furthermore $\bar{f}_i$ can be expressed as:

$$\bar{f}_i = y_i P_{rxn} \phi_i \tag{11}$$

where y_i is the mole fraction of species i, P_{rxn} is the total reaction pressure, and ϕ_i is the fugacity coefficient. Moreover, the fugacity coefficient [21] for 1–5 bars total pressure and temperatures between 500–1000 °C can be approximated to $\phi_i \cong 1$. Thus,

$$\bar{f}_i = y_i P_{rxn} = p_i \tag{12}$$

As a result, the activity coefficient in Eq. (10) for the gas species becomes:

$$a_i = p_i \tag{13}$$

For instance, in the case of calcite in the decarbonation unit, the equilibrium constant, $K_{p,decarbonation1}$, for the CO_2 removal can be expressed as:

$$K_{p,decarbonation1} = \frac{a_{CaO}(p_{CO_2,e})}{a_{CO_3CaO}} \tag{14}$$

where a_{CaO}, a_{CO_3CaO} are activity coefficients of the calcination reaction and $p_{CO_2,e}$ is the partial pressure of CO_2.

Since, the activity coefficients for solids and for the fugacity of the gases at the expected operating conditions are close to one, the equilibrium constant for the calcination unit becomes:

$$K_{p,decarbonation1} = p_{CO_2,e} \tag{15}$$

Similarly, during carbonation, the equilibrium constant can be expressed as:

$$K_{p,carbonation1} = \frac{1}{p_{CO_2,e}} \tag{16}$$

A comparable analysis can be developed for CO_2 removal at equilibrium conditions using Li_4SiO_4. In this case, $K_{p,decarbonation2}$ can be expressed as:

$$K_{p,decarbonation2} = \frac{a_{Li_4SiO_4}(p_{CO_2,e})}{a_{Li_2SiO_3}.a_{Li_2CO_3}} \tag{17}$$

$$Therefore, K_{p,decarbonation2} = p_{CO_2,e} \tag{18}$$

Furthermore, in the case of the Li_4SiO_4 carbonation, the equilibrium constant for carbonation can be calculated as:

$$K_{p,carbonation2} = \frac{1}{p_{CO_2,e}} \tag{19}$$

Similar expressions can be established for calculating decarbonation equilibrium constants for both lithium zirconate and sodium silicates such as: $K_{p,decarbonation3} = p_{CO_2,e}$ and $K_{p,carbonation3} = \frac{1}{p_{CO_2,e}}$.

According to the definition of the standard Gibbs Energy change of reaction, it can be postulated that:

$$\frac{\Delta G^\circ}{RT} = -\ln K \tag{20}$$

Therefore, for CO_2 release i.e. decarbonation, at the equilibrium Eq. (20) can be described as:

$$\Delta G^\circ + RT \ln p_{CO_2} = 0 \tag{21}$$

As a result, Eq. (21) is satisfied at equilibrium for each one of the CO_2 sorbents considered in Eqs. (1)–(4).

One should notice that at initial conditions, in the decarbonation unit, if the partial pressure p_{CO_2} is too low, Eq. (21) becomes negative:

$$\Delta G^\circ + RT \ln p_{CO_2} < 0 \tag{22}$$

This negative value in Eq. (22) occurs when all absorbed CO_2 decomposed in the decarbonation unit but could not reach equilibrium condition.

On the other hand, if p_{CO_2} is high enough in the decarbonation unit, Eq. (21) may become positive:

$$\Delta G^\circ + RT \ln p_{CO_2} > 0 \tag{23}$$

This shows that as long as Eq. (23) is positive, no decomposition of sorbent will occur. Rather carbonation will proceed until CO_2 partial pressure decreases enough so that Eq. (21) is fully satisfied.

3. Thermodynamic model predictions for different sorbents

3.1. Gibbs Energy changes

The Gibbs Free Energy changes can be calculated on the basis of thermodynamic data [22]. Fig. 1 reports the Gibbs Free Energy changes for carbonation and decarbonation for the four sorbents considered in the present study as a function of the temperature and at 1 bar CO_2 partial pressure.

Negative values of Gibbs Energies in Fig. 1 shows conditions where reactions proceed towards the right side of Eqs. (1)–(4) i.e. CO_2 is absorbed. These results suggest that CO_2 can be absorbed even at room temperatures. However, due to kinetic limitations, CO_2 absorption at room temperatures is not viable. Thus, high temperatures are required for adequate CO_2 capture kinetics, with the exothermicity of carbonation reactions also benefiting the CO_2 capture [23]. This is true for lithium orthosilicate, lithium zirconate [6] and calcium oxide [24].

One can notice in Fig. 1, that there are specific temperatures to achieve zero Gibbs Energies for carbonation. These temperatures are 325 °C, 720 °C, 750 °C and 900 °C for sodium silicate, lithium orthosilicate, lithium zirconate and calcite respectively. These temperatures yielding zero Gibbs Energies are designated as "*Inversion Point Temperatures*". One should also note that lower inversion temperatures not only allow CO_2 capture processes with lower energy demands but also help to avoid sorbent sintering. Sintering is one of the main reasons for sorbent deactivation. Preventing sintering is a main factor for sorbent choice.

3.2. Equilibrium partial pressure change

Fig. 2 reports equilibrium partial pressures for CO_2 absorption and CO_2 desorption for several sorbents and their changes with temperature. It shows that Li_4SiO_4 can desorb CO_2 at 560 °C if CO_2 partial pressure is below 0.1 bar. However, if the partial pressure of CO_2 is higher than 0.1 bar, absorption takes place at this temperature.

Fig. 2 also reports that CO_2 capture from hot flue gases (generally 400–800 °C), using lithium orthosilicate, lithium zirconate and calcite is thermodynamically viable. These materials belong to the so-called high temperature CO_2 capture sorbents. From Fig. 2, one can also see that in principle, sorbents such as Li_4SiO_4, Li_2ZrO_3, and $CaCO_3$ are capable of absorbing CO_2 from hot flue gases.

4. Experimental

All the chemicals used in this work were of reagent grade. The 99.9 wt% lithium orthosilicate (Li_4SiO_4), the 99.0 wt% calcium carbonate ($CaCO_3$), and the 94 wt% lithium zirconate (Li_2ZrO_3) were obtained from Alfa Aesar, Massachusetts, USA. The 99.7 v/v% glacial acetic acid (HAc) was from Aldrich Chemical Co., Wisconsin, USA; and the 10 v/v% carbon dioxide with helium being the balance was from Praxair, Canada. All chemicals were used as received without further purification.

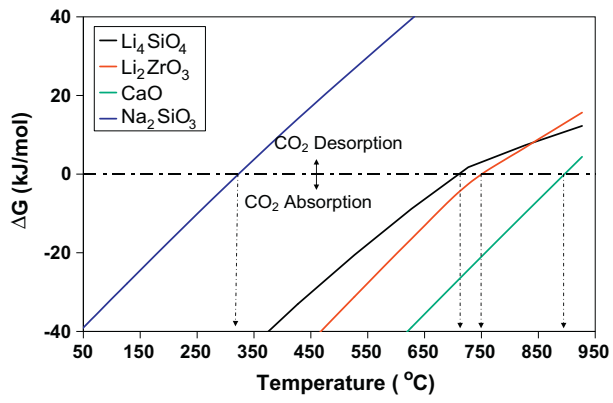

Fig. 1. Temperature dependence of Gibbs Energy of reaction for carbonation and decarbonation reactions (CO_2 partial pressure 1 bar).

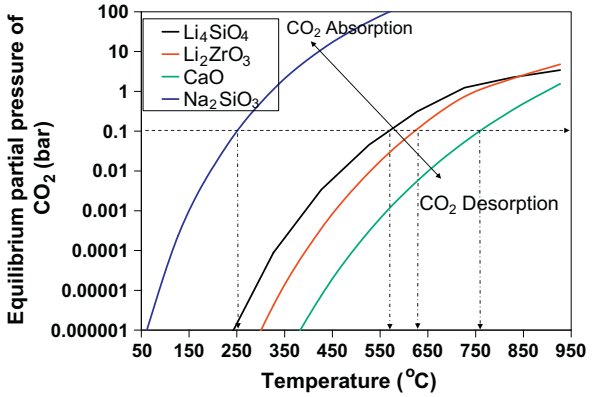

Fig. 2. Equilibrium partial pressure dependence with temperature. Note: reported curves separate the CO_2 absorption conditions (carbonation) and CO_2 desorption (decarbonation) conditions. Broken horizontal line provides the inversion temperature for 0.1 bar equilibrium pressure.

4.1. Preparation of as received solid sorbent

Solid sorbents were thermally treated to increase thermal stability and remove absorbed CO_2, water vapor and other adsorbed gaseous impurities. To achieve this, $CaCO_3$ was calcined at 930 °C while Li_2ZrO_3 and Li_4SiO_4 were calcined at 675 °C under atmospheric condition. Conditions for pre-treatment for sorbent calcinations were set to exceed considerably the equilibrium temperatures. As reported in Fig. 2 for a 0.00039 bar CO_2 partial pressure in air these equilibrium temperatures were: 527 °C for CaO, 427 °C for Li_2ZrO_3 and 374 °C for Li_4SiO_4.

4.2. Preparation of the novel fluidizable solid sorbent

The preparation of the new fluidizable solid sorbent involves the following steps: (a) Li_4SiO_4 is mixed with glacial HAc excess (molar ratio is 1:10) followed by continuous stirring. (b) After mixing, a packed bed of precursor sorbent particles is calcined under nitrogen flow from room temperature to 620 °C in 2 h. (c) Following calcination, the sorbent particles are exposed to a helium flow at 675 °C for 1 h. This allows the removal of any carbonaceous species or gaseous products remaining adsorbed on the sorbents.

4.3. Sorbent characterization

Sorbent characterization was developed using the Brunauer–Emmett–Teller (BET) surface area, pore size and distribution, and pore volume from nitrogen absorption and desorption isotherms at 77 K. A constant-volume absorption apparatus (Micromeritics ASAP 2010) using N_2 gas (99.995% pure; obtained from Praxair, Canada) was utilized. The prepared samples were degassed at 150 °C for 6 h before measurements were taken. Micromeritics' DFT Plus software for Windows™ was used to calculate pore volume and pore size distribution by applying 'Density Functional Theory' (DFT) based on slit-shape pore geometry.

X-ray diffraction (XRD) patterns of catalysts were obtained to establish crystallinity and crystallinity changes, given that its importance on sorbent performance. XRD was performed utilizing a Rigaku Difractometer (Ultima IV) unit with a CuKα1 + Kα2 equal to 1.54184 Å radiation. The XRD instrument was operated at 45 kV and 160 mA, using the normal scan rate of 10° per minute (equivalent to 0.5° two-theta on conventional diffractometers) in the 2θ range spanning from 10° to 90°. X-rays were collimated using 1° divergent and scatter slits, and a 0.2 mm receiving slit. XRD peaks were identified in the present study, using a Rigaku Difractometer

(Ultima IV) and the 'International Center for Diffraction Data' library. Crystallinity was defined for each one of the analyzed samples using the following equation:

$$Crystallinity = \frac{Scattered\ intensity\ from\ crystalline\ phase}{Scattered\ intensity\ from\ crystalline\ phase + Scattered\ intensity\ from\ amorphous\ phase}$$

The CO_2 absorption–desorption sorbent capacity and the "inversion temperature" were established using Temperature Programmed Carbonation–Decarbonation (TPC-TPDC). The TPC-TPDC experiments were carried out using a Micromeritics Autochem 2920. Prior to TPC measurements, 100–150 mg of the fresh sorbent was calcined at 675 °C under a helium flow to remove moisture, entrap CO_2 and other loosely bonded impurities. The TPC runs were performed by circulating a stream of gas containing 10% CO_2 with He making the balance at a rate of 50 mL/min. The temperature was raised from ambient to the required temperature at a rate of 5 °C/min.

A Thermal Conductivity Detector (TCD) was used to record the change in carbon dioxide concentration in the gas stream exiting the bed of sorbent. CO_2 amounts were recorded at the sorbent bed exit and used to calculate the carbon dioxide consumed or released during the carbonation and decarbonation (regeneration).

5. Results and discussions

5.1. Surface area and pore size distribution

Surface area, average pore diameter and pore volume of the sorbents of the present study are summarized in Table 1.

It can be observed in Table 1 that the specific surface area of $CaCO_3$ increased with calcination. This gain in specific surface area can be attributed to the CO_2 release from $CaCO_3$. Regarding limestone (Cadomin 1), the specific surface area also augmented significantly with calcination. However, pore volume remained low for both $CaCO_3$ and limestone, even after calcination.

Concerning lithium zirconate and untreated lithium orthosilicate, calcination led to significant reductions of surface area. More specifically, when using untreated lithium orthosilicate, there was both a reduction of pore volume and surface area, with this being attributed to the collapse of the pore sorbent network. Finally, calcinations of glacial acetic acid treated Li_4SiO_4, retained both a significant fraction of surface area and pore volume. This result is consistent with the observed lower apparent density of the acid treated Li_4SiO_4 (0.98 g/cm^3). This is also the case with respect to the higher apparent density of untreated Li_4SiO_4 (1.24 g/cm^3).

Fig. 3a and b compare the nitrogen adsorption–desorption isotherms and the corresponding pore size distributions of sorbents after calcination. Isotherm shapes and hysteresis loops are those of 'type IV' isotherms with H3 and H4 loops [25]. CaO and untreated Li_4SiO_4 show small H3 loops, confirming that these materials are mostly nonporous with some slit-like pores [25]. On the other hand, large H4 loops are observed for the acid treated Li_4SiO_4, suggesting the presence of large irregular shaped mesopores and a broad pore size distribution with slit like pores [25].

Fig. 4a and b compare isotherms and pore size distributions for both carbonated and decarbonated sorbents. Reported pore size distributions were calculated using the 'Density Functional Theory' model (DFT model) based on slit-shape pore geometry. The shape of the isotherms and their hysteresis loops remained close. However, as shown in Fig. 4b, there was a reduction in pore volume in carbonated sorbents attributed to CO_2 absorption. Fig. 4b also reports a comparatively larger pore size distribution and pore volume, with this being consistent with the findings for acid treated Li_4SiO_4. Thus, pore size distributions show that the acid treated Li_4SiO_4 provides a stable sorbent, with a pore network providing good CO_2 accessibility even under carbonated conditions.

Table 1
Physiochemical properties of the sorbents.

Catalysts	BET surface area (m^2/gm)			Average pore diameter (Å)			Pore volume (cm^3/gm)		
	Fresh	Calcined	After 10 cycle	Fresh	Calcined	After 10 cycle	Fresh	Calcined	After 10 cycle
$CaCO_3$	3.08	5.05	–	22.0	49.7	–	0.002	0.006	–
Limestone	3.49	9.83	3.93	24.6	93.9	115.4	0.002	0.023	0.011
Li_2ZrO_3	6.37	2.24	–	43.2	16.4	–	0.007	0.001	–
Li_4SiO_4	36.74	4.73	2.82	167.3	39.5	107.3	0.154	0.005	0.004
Li_4SiO_4/HAc	–	9.35	7.21	–	85.9	104.9	–	0.020	0.015

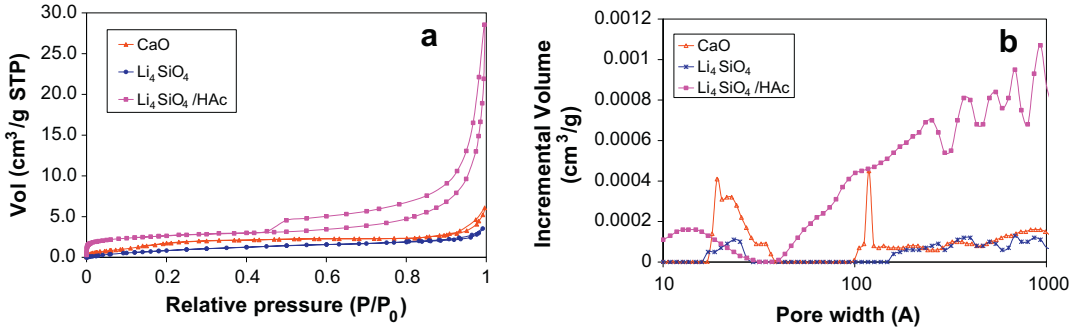

Fig. 3. (a) N_2 adsorption/desorption isotherms and (b) pore-size distributions of calcined sorbents. (Δ) Fresh calcium oxide calcined at 930 °C, (∗) lithium orthosilicates calcined at 650° C, (■) HAc treated Lithium orthosilicates calcined at 650° C.

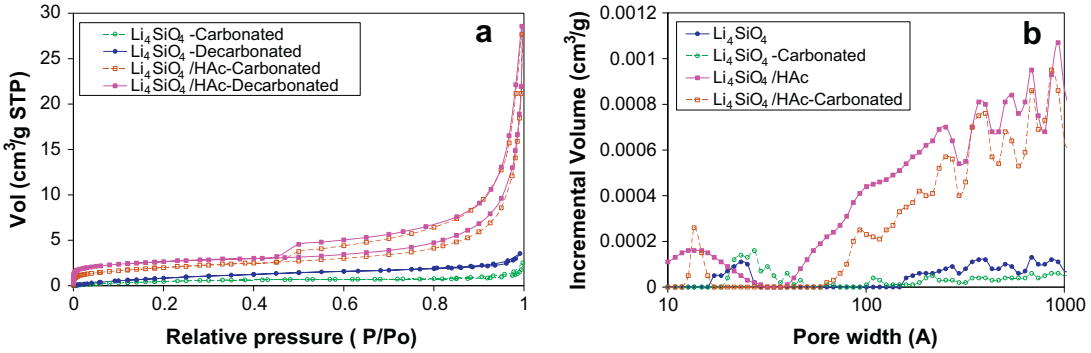

Fig. 4. (a) N_2 adsorption/desorption isotherms and (b) pore-size distributions for carbonated and decarbonated sorbents.

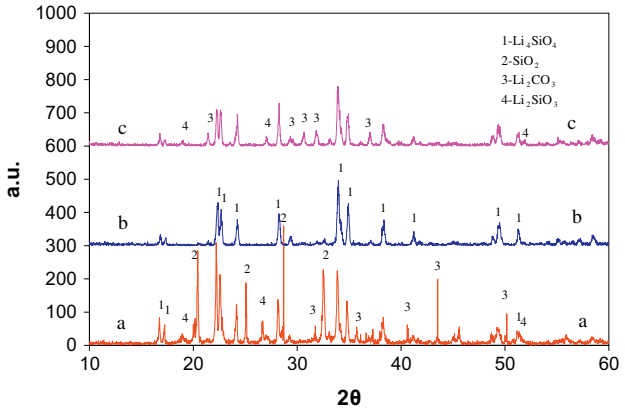

Fig. 5. XRD diffractogram: (a) as received Li_4SiO_4, (b) calcined Li_4SiO_4 675 °C, and (c) Li_4SiO_4 after 10 absorption–desorption cycles.

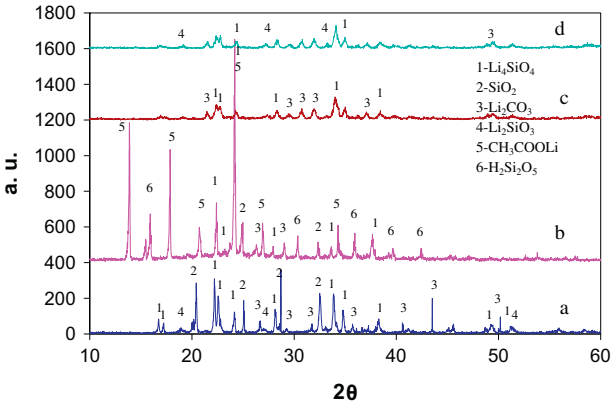

Fig. 6. XRD diffractogram for: (a) As received Li_4SiO_4, (b) acid treated Li_4SiO_4 (dried at room temperature). (c) Acid treated calcined Li_4SiO_4 and (d) after 10 cycles of CO_2 absorption–desorption with acid treated Li_4SiO_4.

5.2. XRD analysis

XRD allows the identification of various crystalline phases on Li_4SiO_4 and on Li_4SiO_4 pre-treated with acetic acid as shown in Fig. 5. It was observed that the Li_4SiO_4 sample as received contained crystalline Li_2CO_3, Li_2SiO_3 and SiO_2 phases. Upon calcination at 675 °C however, these phases disappear, forming additional lithium orthosilicate. As a result, the following reactions can be considered to occur:

$$2Li_2CO_3 + SiO_2 \rightarrow Li_4SiO_4 + 2CO_2 \quad (24)$$

$$Li_2CO_3 + Li_2SiO_3 \Longleftrightarrow Li_4SiO_4 + CO_2 \quad (25)$$

However, after repeated CO_2 absorption–desorption cycles, the characteristic Li_2CO_3 and Li_2SiO_3 peaks re-appeared (reverse reaction of Eq. (25)) confirming that the regeneration process of the Li_4SiO_4 sorbent remained incomplete. This was likely due to the diffusion resistance consequence of pore blockage and the formation of core-shell structures of Li_2CO_3 and Li_2SiO_3 on the sorbent.

Acetic acid treatment of Li_4SiO_4, however, initially created crystalline lithium acetate salts and silicic acids, as shown in Fig. 6. A possible reaction leading to the formation of acetate salts can be considered as follows:

$$2Li_4SiO_4 + 8CH_3COOH \rightarrow 8CH_3COOLi + H_2Si_2O_5 + 3H_2O \quad (26)$$

Silicic acid and in situ water undergo polycondensation following the sol gel process forming polymeric three dimensional networks [26]. This network may remain even after calcinations, helping to increase the sorbent porosity.

After calcination of the acid treated sorbent however, the formed acetate salts are converted mainly into porous lithium orthosilicates. This can be supported by observing the disappearance all peaks of type "5" in the "c" diffractogram of Fig. 6. One can also observe that lithium silicates are less intense using an acid treated sorbent. However, peaks of $LiCO_3$ appear to also be prominent in the "c" diffractogram while Li_2SiO_3 is insignificant. Thus, from these observations, the following reactions appear to occur during calcination of acid treated Li_4SiO_4 sorbents:

$$2CH_3COOLi \rightarrow Li_2CO_3 + CH_3COCH_3 \quad (27)$$

$$H_2Si_2O_5 + 3Li_2CO_3 \rightarrow Li_4SiO_4 + Li_2SiO_3 + H_2O + CO_2 \quad (28)$$

$$Li_2SiO_3 + Li_2CO_3 \rightarrow Li_4SiO_4 + 2CO_2 \quad (29)$$

One can thus see that when comparing untreated Li_4SiO_4 with acetic acid treated Li_4SiO_4, the Li_4SiO_4 microstructure is significantly altered by the acetic acid addition. There is also, significant re-crystallization of Li_4SiO_4, as shown in Fig. 6b after acetic acid addition. One can also notice that after acetic acid treatment followed by calcination, the dominant Li_4SiO_4 peaks appear again in the XRD difractograms with these peaks being observed at lower intensities. Moreover, after repeated cycles of operation, the dominant peaks remain with similar approximate intensities confirming the stability of the acid treated Li_4SiO_4 sorbent.

Fig. 5b and c report XRD analysis for calcined Li_4SiO_4 and Li_4SiO_4 after 10 absorption–desorption cycles. One can see comparing these two figures that there is an increase in the Li_2CO_3 content. On this basis one can claim that changes in sorption activity can be expected due to incomplete sorbent regeneration. Fig. 6c and d shows that on the other hand, in the case of acid treated Li_4SiO_4, the Li_2CO_3 content (Eq. (27)) remains steady for both calcined Li_4SiO_4 (Fig. 6c) and Li_4SiO_4 after 10 repeated cycles (Fig. 6d).

XRD was also valuable to establish the changes in crystallinity during the pre-treatment process. For instance, Fig. 5b shows that Li_4SiO_4 was 82% crystalline following calcination at 675 °C. On the other hand, once the lithium orthosilicate sorbent is treated with glacial acid acid, there is an increased crystallinity up to 96% due to the formation of acetate salt as shown in Fig. 6b. Formed acetate salts are converted however into porous lithium orthosilicates upon calcination with reduced crystallinity to 64% (Fig. 6c).

As a result, the acetic acid addition leads to Li_4SiO_4 sorbents with enhanced pore structure with a higher pore volume, a wider pore size distribution and reduced particle density.

5.3. Performance evaluation with Temperature Programmed Carbonation–Temperature Programmed Decarbonation (TPC–TPDC)

TPC–TPDC is a valuable experimental tool for establishing the following: (a) the CO_2 absorption and desorption capacity of a sorbent and its evolution with carbonation–decarbonation sequential cycles, (b) the inversion temperature or the temperature where the sorbent interaction with CO_2 is neither in the absorption mode nor in desorption mode, (c) the kinetics of CO_2 absorption/desorption.

As stated above, the temperature ramp selected for the present study was 5 °C/min. This temperature ramp allows increasing the temperature to 100 °C in about 20 min. This is the typical solid residence time that one can expect in large scale dense fluidized beds using this type of sorbent material. Thus, these CO_2 absorption–desorption capacity results were obtained under dynamic conditions with a sorbent time-on-stream of 15–20 min. These times-on-stream are close to the times-on-stream expected in a twin reactor configuration involving CO_2 absorption and desorption in large scale fluidized bed units".

Fig. 7 reports three interesting absorption–desorption (carbonation–decarbonation) cases. One can see that when using a commercial calcite, with a CO_2 partial pressure of 0.1 bar, the CO_2 is continuously absorbed until the temperature reaches 722 °C. This thermal level (thermal inversion point) is in agreement with thermodynamics predicting 750 °C for this same condition.

In the case of calcite, a maximum Temperature Programmed Carbonation (TPC) peak is obtained at 665 °C while the desorption of CO_2 starts only after 722 °C. On the other hand, the desorption peak displays a maximum Temperature Programmed Decarbonation (TPDC) at 768 °C reaching a plateau above 810 °C. Thus, this shows that the CO_2 desorption processes require very high temperatures to be completed.

For Li_2ZrO_3, only a partial absorption peak ending at 700 °C and no desorption peak were observed. As described earlier, temperature could not be raised above 720 °C. This was due to the melting point of Li_2CO_3, which is one of the products formed by absorbing CO_2 on Li_2ZrO_3. Thus, Li_2ZrO_3 could not be regenerated. Therefore, Li_2ZrO_3 is considered unsuitable for CO_2 capture from hot flue gases.

On the other hand, when using Li_4SiO_4, TPC–TPDC curves display promising results in terms of CO_2 absorption and desorption at lower temperatures than the other sorbents considered in the present study. CO_2 is absorbed below the 595 °C inversion temperature condition with a maximum TPC peak at 567 °C. This thermal level (inversion point temperature) established with a heating ramp of 5 °C/min is in agreement with the thermodynamics which predicts 575 °C at 0.1 bar CO_2 partial pressure. Moreover, close "inversion point temperatures" were also obtained in separate runs performed using 2.5 °C/min, 7.5 °C/min and 10 °C/min temperature ramps. Deviations remained in the ±2 °C range.

Regarding the Li_4SiO_4 carbonation process, one can observe a double peak. This double peak is assigned to the formation of outer shell structures consisting of Li_2CO_3 and Li_2SiO_3 [17]. In fact, while CO_2 chemisorption controls the reactivity of Li_4SiO_4 during CO_2 absorption at the initial carbonation stages (first peak), once an external lithium shell is formed the absorption process likely becomes diffusionally controlled (second peak). Under these conditions, higher TPC temperatures are required for full Li_4SiO_4 carbonation.

CO_2 absorption–desorption processes using Li_4SiO_4 however, have to be limited to thermal levels below 720 °C. This is due to the melting point of Li_2CO_3. To compensate for this and to complete the TPC–TPDC, the sorbent temperature was held at 700 °C for an hour.

Fig. 7 also shows that Li_4SiO_4 and CaO display good agreement between thermodynamics and experimental findings for the "inversion point temperature. However, Li_2ZrO_3 with 94 wt% purity display a significant difference between the equilibrium "inversion point temperature" and the practical observed value. Even at the Li_2CO_3 melting temperature (720 °C), the "inversion point temperature" for Li_2ZrO_3 is still not reached.

Furthermore, for cyclic use in CO_2 capture, sorbents need to be regenerated. In this respect, Li_4SiO_4 requires a lower regeneration temperature when compared to CaO. The difference of equilibrium "inversion point temperatures" between CaO and Li_4SiO_4 is approximately 180 °C. Regarding Li_4SiO_4 and Li_2ZrO_3, while Li_4SiO_4 display a 30 °C lower inversion temperature than Li_2ZrO_3 this difference is in practice much larger (>110 °C).

Fig. 8 shows the CO_2 absorption using commercial calcite (99.98%) and limestone (Cadomin 1). Although both are CaO based

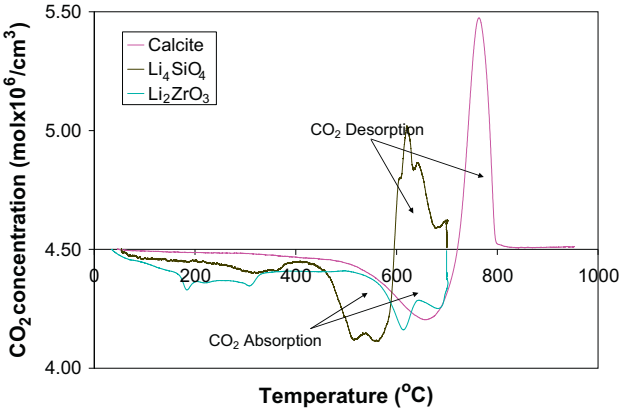

Fig. 7. The CO_2 absorption–desorption cycle with respect to temperature (Temperature ramp: 5 °C/min; Input Gas composition: 10 vol% CO_2 in helium; flow rate: 50 mL/min).

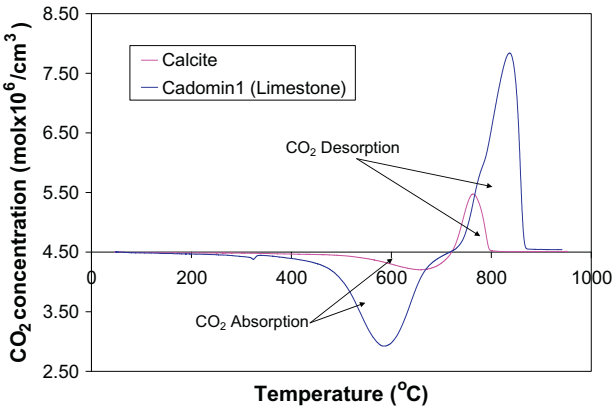

Fig. 8. CO_2 absorption–desorption with temperature by calcite and Cadomin 1 (limestone). (Temperature ramp: 5 °C/min; Input Gas composition: 10 vol% CO_2 in helium; flow rate: 50 mL/min).

sorbents, Cadomin1 contains 53 wt% CaO only. It can be noticed, in this respect, that CaO doping with other materials such as MgO may help to increase CO_2 capacity. For instance, it can be observed that Cadomin1 has a comparatively higher surface area and higher porosity than calcite. These two morphological parameters may affect CO_2 absorption and desorption.

It can also be noticed that the inversion temperature, was unaffected by the CaO specific composition. This is the case since the inversion temperature is a thermodynamic property which remains unchanged for calcite and Cadomin 1, at 700 °C and 710 °C respectively.

6. Sorbent stability studies

Figs. 9 and 10 display the CO_2 sorbent capacity for CO_2 capture over repeated cycles at approximately 0.1 bar partial pressure of CO_2. It has already been discussed in the present study that at a constant partial pressure of CO_2, the absorbed CO_2 is desorbed if the temperature is increased beyond an equilibrium thermal level. This so-called "temperature inversion" point, as reported in Figs. 9 and 10 remains almost constant over repeated absorption–desorption cycles. This predictability of "temperature inversion" points confidently supports the soundness of the thermodynamic analysis described earlier.

Furthermore, one can also notice in both Figs. 9 and 10, that the sorbent absorption capacity of both limestone and lithium orthosilicate decreases over repeated cycles. As shown with XRD, the appearance of new phases after CO_2 absorption–desorption cycles suggest partial decomposition of Li_4SiO_4. This decay of absorption capacity can be assigned to sorbent sintering and losses of sorbent surface area, with a significant reduction of the mesopore-small pore volume necessary for carbonate product storage.

As described earlier, to improve absorption stability, a novel fluidizable Li_4SiO_4 based sorbent was developed. Fig. 11 reports the CO_2 absorption–desorption capacity of the novel Li_4SiO_4 for over repeated cycles. One can see that the absorption capacity of Li_4SiO_4 did not change significantly over repeated cycles, confirming the stability of the acetic acid treated Li_4SiO_4. It is postulated that acetic acid modifies the microstructure of Li_4SiO_4, resulting in a more stable sorbent. In this respect, Li et al. assumed that an acetic acid solution leads to a better sorbent sintering resistance given that modified limestone protects CaO grain growth [27].

Fig. 12 provides a comparison of sorbent efficiencies using the following efficiency definition:

$$= \frac{\textit{Experimental } CO_2 \textit{ uptake}}{\textit{Maxium } CO_2 \textit{ uptake as } Li_4SiO_4 \textit{ expected by stoichiometry}} \times 100\% \quad (30)$$

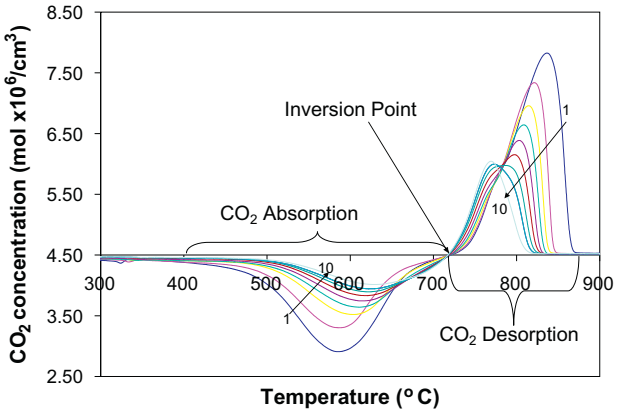

Fig. 9. The CO_2 absorption–desorption (10 cycles) profile of limestone with respect to temperature. (Temperature ramp: 5 °C/min; Input Gas composition: 10 vol% CO_2 in helium; flow rate: 50 mL/min). Note: direction of the arrows describes successive runs: from run 1–10.

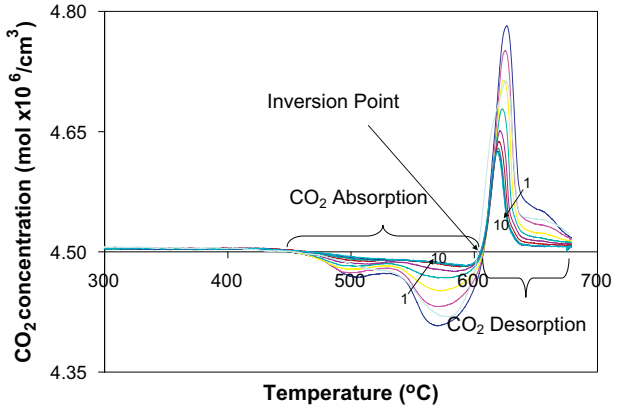

Fig. 10. The CO_2 absorption–desorption (10 cycles) profile of Li_4SiO_4 with respect to temperature. (Temperature ramp: 5 °C/min; Input Gas composition: 10 vol% CO_2 in helium; flow rate: 50 mL/min). Note: direction of the arrows describes successive runs: from run 1–10.

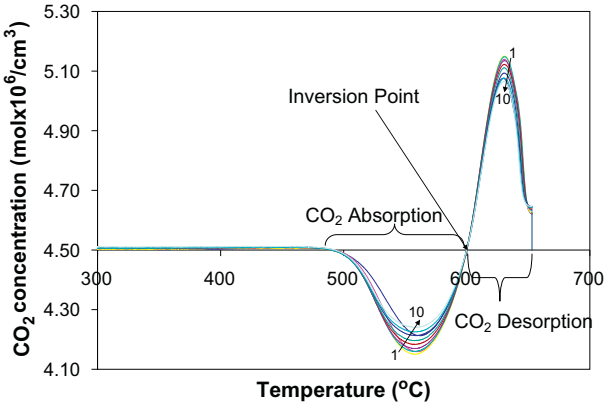

Fig. 11. The CO_2 absorption–desorption (10 cycles) profile of modified Li_4SiO_4 with respect to temperature (Temperature ramp: 5 °C/min; Input Gas composition: 10 vol% CO_2 in helium; flow rate: 50 mL/min). Note: direction of the arrows describes successive runs: from run 1–10.

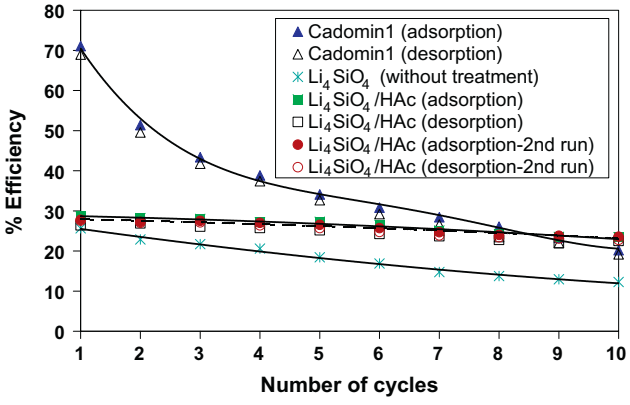

Fig. 12. The CO_2 absorption–desorption efficiencies over repeated cycles. (Closed symbols are for absorption and open symbols are for desorption).

It can be noticed that although Cadomin1 shows a higher sorbent efficiency than Li_4SiO_4 during the initial cycles of absorption–desorption, the Cadomin1 sorbent efficiency as defined in Eq. (30), drops drastically over repeated cycles.

Table 2 shows the quantitative information of CO_2 uptake and release during cyclic process. Li_4SiO_4 without acid treatment showed a moderate CO_2 capacity reduction over absorption–desorption repeated cycles: from 48.3 mL/gm in cycle one to 23.1 mL/gm in cycle ten. This CO_2 reduced capacity was assigned to diffusional resistance effects, which are the result of the formation of a core shell structure. On the other hand, acid treated Li_4SiO_4 increases the fraction of mesopores preventing the formation of the core shell structure. This yields as a result a more stable sorbent, exceeding even Cadomin1 efficiency in the 9th cycle.

Fig. 13 also compares the theoretical and experimental "temperature inversion" conditions and thermal levels where CO_2 absorption and desorption rates are in balance. One can notice a consistency between the theoretical values as expected by thermodynamics and the experimental data. These predictions which are approximately similar to each other are valuable, given that they allow setting adequate conditions for a twin configuration involving absorption and desorption fluidized bed units.

Table 2
Quantitative capacity of the sorbents.

Cycle	Limestone		Li_4SiO_4		Li_4SiO_4/HAc	
	CO_2 captured (mL/gm)	CO_2 released	CO_2 captured (mL/gm)	CO_2 released	CO_2 captured (mL/gm)	CO_2 released
1	151.6	147.1	48.3	46.9	52.3	51.9
2	109.6	105.7	43.1	41.9	51.3	50.9
3	92.5	89.1	40.9	39.1	51.8	51.1
4	82.8	79.8	38.8	37.5	50.9	49.7
5	72.7	69.7	34.7	33.5	49.9	48.4
6	65.7	62.3	31.8	30.2	48.4	46.6
7	60.6	56.7	27.8	26.4	46.5	45.0
8	55.6	50.1	25.9	23.7	45.2	44.1
9	49.8	46.9	24.4	22.9	44.8	43.5
10	43.1	40.9	23.1	21.1	44.4	42.9

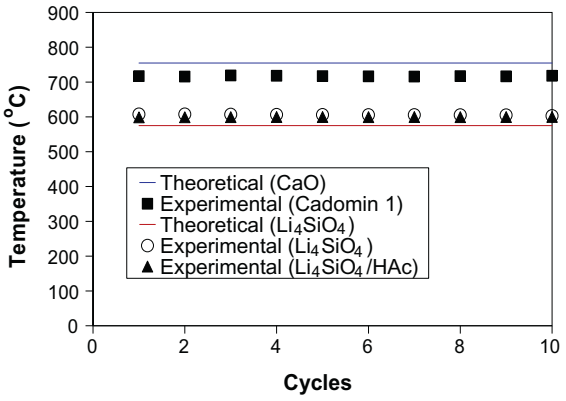

Fig. 13. Theoretical and experimental "inversion point temperature" for CO_2 absorption–desorption at the partial pressure of 0.1 bar. Full line: CaO theoretical "inversion point temperature", broken line: theoretical "inversion point temperature" for Li_4SiO_4, (■) experimental "inversion point temperature" for Cadomin 1, (○) experimental "inversion point temperature" for Li_4SiO_4, (Δ) experimental "inversion point temperature" for Li_4SiO_4 pretreated with acetic acid.).

7. Conclusions

(1) It is shown that gas–solid sorption thermodynamics helps to predict sorbent regeneration conditions, and the temperatures where sorbent kinetics change from CO_2 absorption to CO_2 desorption.
(2) It is observed that Temperature Programmed Carbonation (TPC) and Temperature Programmed Decarbonation (TPDC) help to establish absorption–desorption performance for several CO_2 sorbents.
(3) It is noticed that limestone absorption capacity is drastically reduced over repeated cycles while modified Li_4SiO_4 is stable and reproducible.
(4) It is found that an acid treated fluidizable Li_4SiO_4, provides a promising sorbent for CO_2 capture with increased specific surface area, higher porosity and stable sorbent capacity.

Acknowledgments

We would like to thank the financial support of the Carbon Management Canada who provided a Post-Doctoral fellowship to Dr. Muhammad B.I. Chowdhury. We would also like to acknowledge the Natural Sciences and Engineering Research Council of Canada for the financial support of the research. Authors would also like to acknowledge Ms F. de Lasa for her assistance during the preparation of this manuscript.

Appendix A. Thermodynamic properties of the CO_2 sorbents studied

A.1. Heat capacity of various chemical species

Heat capacities of the various chemical species were defined in J/mol-K [28–31] with the temperature, T involved in the following correlations given in degrees Kelvin:

$$C_{p\ CO_2} = 22.243 + 5.977 \times 10^{-2}T - 3.499 \times 10^{-5} + 7.464 \times 10^{-9}$$

$$C_{p\ CaCO_3} = 82.34 + 0.0497T - 1287000/T^2$$

$$C_{p\ CaO} = 41.84 + 0.02025T - 451870/T^2$$

$$C_{p\ LiCO_3} = 68.33 + 146.610^{-3}T - 162.510^{-6}T^2 + 248.010^{-9}T^3 - 0.70210^6T^2[298 - 683\ \mathrm{K}]$$

$$C_{p\ LiCO_3} = -6.394 + 261.410^{-3}\mathrm{T} - 102.010^{-6}T^2 + 42.4710^{-9}T^3 - 0.16810^6T^2[683\ \mathrm{K} - 993\ \mathrm{K}]$$

$$C_{p\ ZrO_2} = 69.20 + 8.5410^{-3}T - 0.86210^{-6}T^2 + 0.24610^{-9}T^3 - 1.38210^6/T^2$$

$$C_{p\ Li_2ZrO_3} = 125.81 + 47.7110^{-3}T - 25.78 \times 10^5/T^2$$

$$C_{p\ Li_2SiO_3} = 171.3 + 18.8210^{-3}T - 17.6610^5/T^2 - 971.4/T^{-1/2}$$

$$C_{p\ Li_4SiO_4} = 1160.1 + 0.401T - 3.263 \times 10^6/T^2$$

A.2. Standard Gibbs Free Energies and standard enthalpies for various chemical reactions

Table A reports the standard Gibbs Free Energies and the standard heat of reaction for the various chemical species involved in the calculations of the present study [22].

Table A
Standard Gibbs free energies and standard heat of enthalpies for various reactions.

	ΔG_R°(kJ/mole)	ΔH_R°(kJ/mole)
$CO_3Ca \Longleftrightarrow CaO + CO_2$	130.9	178.3
$SiO_3Li_2 + Li_2CO_3 \Longleftrightarrow LiSiO_4 + CO_2$	92.83	141.97
$CO_3Li_2 + ZrO_2 \Longleftrightarrow Li_2ZrO_3 + CO_2$	110.6	159.8
$Na_2CO_3 + SiO_2 \rightarrow Na_2SiO_3 + CO_2$	42.66	86.614

References

[1] J.G. Canadell, C. Le Quéré, M.R. Raupach, C.B. Field, E.T. Buitenhuis, P. Ciais, T.J. Conway, N.P. Gillett, R.A. Houghton, G. Marland, Contributions to accelerating atmospheric CO_2 growth from economic activity, carbon intensity, and efficiency of natural sinks, Proc. Natl. Acad. Sci. 104 (2007) 18866–18870.

[2] H. Gupta, L.S. Fan, Carbonation–calcination cycle using high reactivity calcium oxide for carbon dioxide separation from flue gas, Ind. Eng. Chem. Res. 41 (2002) 4035–4042.

[3] J.R. Grace, A.A. Avidan, T.M. Knowlton, Circulating Fluidized Beds, Blackie Academic and Professional, London, UK, 1997.

[4] M.A. Cuenca, E.J. Anthony, Pressurized Fluidized Beds, Blackie Academic & Professional, Glasgow, U.K., 1995.

[5] L.I. Eide, M. Anheden, A. Lyngfelt, C. Abanades, M. Younes, D. Clodic, A.A. Bill, P.H.M. Feron, A. Rojey, F. Giroudiere, Novel capture processes, Oil Gas J. Sci. Technol. 60 (2005) 497–508.

[6] J. Ida, R. Xiong, Y.S. Lin, Synthesis and CO_2 sorption properties of pure and modified lithium zirconate, Sep. Purif. Technol. 36 (2004) 41–51.

[7] K. Yi, D. Eriksen, Low temperature liquid state synthesis of lithium zirconate and its characteristics as a CO_2 sorbent, Sep. Sci. Technol. 41 (2006) 283–296.

[8] Y. Duan, Electronic structural and electrochemical properties of lithium zirconates and their capabilities of CO_2 capture: a first-principles density-functional theory and phonon dynamics approach, J. Renewable Sustainable Energy 3 (2011) 013102.

[9] K. Essaki, M. Kato, H. Uemoto, Influence of temperature and CO_2 concentration on the CO_2 absorption properties of lithium silicate pellets, J. Mater. Sci. 40 (2005) 5017–5019.

[10] D.Y. Lu, R.W. Hughes, E.J. Anthony, Ca-based sorbent looping combustion for CO2 capture in pilot-scale dual fluidized beds, Fuel Process. Technol. 89 (2008) 1386–1395.

[11] J. Blamey, E.J. Anthony, J. Wang, P.S. Fennell, The calcium looping cycle for large-scale CO_2 capture, Prog. Energy Combust. Sci. 36 (2010) 260–279.

[12] M. Kato, S. Yoshikawa, K. Nakagawa, Carbon dioxide absorption by lithium orthosilicate in a wide range of temperature and carbon dioxide concentrations, J. Mater. Sci. Lett. 21 (2002) 485–487.

[13] Y. Duan, K. Parlinski, Density functional theory study of the structural, electronic, lattice dynamical, and thermodynamic properties of Li_4SiO_4 and its capability for CO_2 capture, Phys. Rev. B 84 (2011) 104113.

[14] M. Seggiani, M. Puccini, S. Vitolo, High-temperature and low concentration CO_2 sorption on Li_4SiO_4 based sorbents: study of the used silica and doping method effects, Int. J. Greenhouse Gas Control 5 (2011) 741–748.

[15] K. Wang, X. Guo, P. Zhao, F. Wang, C. Zheng, High temperature capture of CO_2 on lithium-based sorbents from rice husk ash, J. Hazard. Mater. 189 (2011) 301–307.

[16] M. Olivares-Marin, T.C. Drage, M.M. Maroto-Valer, Novel lithium-based sorbents from fly ashes for CO_2 capture at high temperatures, Int. J. Greenhouse Gas Control 4 (2010) 623–629.

[17] Z. Qi, H. Daying, L. Yang, Y. Qian, Z. Zibin, Analysis of CO_2 sorption/desorption kinetic behaviors and reaction mechanisms on Li_4SiO_4, AlChE J. (2012). doi: 10.1002/aic.13861.

[18] J. Ortiz-Landeros, T.L. Ávalos-Rendón, C. Gómez-Yáñez, H. Pfeiffer, Analysis and perspectives concerning CO_2 chemisorption on lithium ceramics using thermal analysis, J. Therm. Anal. Calorim. 108 (2012) 647–655.

[19] R. Rodríguez-Mosqueda, H. Pfeiffer, Thermokinetic analysis of the CO_2 chemisorption on Li4SiO4 by using different gas flow rates and particle sizes, J. Phys. Chem. A 114 (2010) 4535–4541.

[20] J.W Tester, M. Modell, Thermodynamics and its Application, 3rd ed., Prentice Hall PTR, New Jersey, USA, 1997.

[21] K. Annamalai, I.K. Puri, Advanced Thermodynamics Engineering, CRC Press LLC, New York, 2002.

[22] I. Barin, Thermochemical Data of Pure Substances, VCH, Newyork, 2008.

[23] V.L. Mejia-Trejo, E. Fregoso-Israel, H. Pfeiffer, Textural, structural, and CO_2 chemisorption effects produced on the lithium orthosilicate by its doping with sodium ($Li_{4-x}Na_xSiO_4$), Chem. Mater. 20 (2008) 7171–7176.

[24] D.K. Lee, An apparent kinetic model for the carbonation of calcium oxide by carbon dioxide, Chem. Eng. J. 100 (2004) 71–77.

[25] M. Kruk, M. Jaroneic, Gas adsorption characterization of ordered organic–inorganic nanocomposite materials, Chem. Mater. 13 (2001) 3169.

[26] S.A. Greenberg, D. Sinclair, The polymerization of silicic acid, J. Phys. Chem. 59 (1955) 435–440.

[27] Y. Li, C. Zhao, H. Chen, C. Liang, L. Duan, W. Zhou, Modified CaO-based sorbent looping cycle for CO_2 mitigation, Fuel 88 (2009) 697–704.

[28] M.W. Chase Jr., NIST-JANAF themochemical tables, J. Phys. Chem. Ref. Data (1998) 1–1951.

[29] G.K. Moiseev, N.A. Vatolin, Interaction of lithium zirconates with lithium under equilibrium conditions, Dokl. Phys. Chem. 388 (2003) 33–37.

[30] M. Asou, T. Terai, Y. Takahashi, High-temperature enthalpy-increment measurements and derived heat capacity of lithium orthosilicate (Li_4SiO_4) at temperatures from 300 K to 1000 K, J. Chem. Thermodyn. 24 (1992) 273–280.

[31] C. Tequi, P. Grinspan, P. Richet, Thermodynamic properties of alkali silicates: heat capacity of Li_2SiO_3 and lithium bearing melts, J. Am. Ceram. Soc. 75 (1992) 2601–2604.